Three-dimensional direct numerical simulation of free-surface magnetohydrodynamic wave turbulence

Evgeny Kochurin,[1,2,*] Guillaume Ricard,[3] Nikolay Zubarev,[2,4] and Eric Falcon[3,†]

[1] *Skolkovo Institute of Science and Technology, 121205, Moscow, Russia*
[2] *Institute of Electrophysics, Ural Division, Russian Academy of Sciences, 620016, Yekaterinburg, Russia*
[3] *Université Paris Cité, CNRS, MSC Laboratory, UMR 7057, F-75013 Paris, France*
[4] *Lebedev Physical Institute, Russian Academy of Sciences, 119991, Moscow, Russia*

(Dated: May 17, 2022)

We report on three-dimensional direct numerical simulation of wave turbulence on the free surface of a magnetic fluid subjected to an external horizontal magnetic field. A transition from capillary-wave turbulence to anisotropic magneto-capillary wave turbulence is observed for an increasing field. At high enough field, wave turbulence becomes highly anisotropic, cascading mainly perpendicularly to the field direction, in good agreement with the prediction of a phenomenological model, and with anisotropic Alfvén wave turbulence. Although surface waves on a magnetic fluid are different from Alfvén waves in plasma, a strong analogy is found with similar wave spectrum scalings and similar magnetic-field dependent dispersionless wave velocities.

Introduction.— Most of nonlinear wave systems reach a wave turbulence regime as a result of wave interactions [1, 2]. This phenomenon occurs in various domains at different scales such as ocean surface waves, plasma waves, hydroelastic or elastic waves, internal or inertial waves, and optical waves [2]. The weakly nonlinear theory (called weak turbulence theory) derived analytically the solutions of the corresponding kinetic equations [1–5]. These solutions, known as the Kolmogorov-Zakharov (KZ) spectra, describe the energy transfers towards small scales (direct cascade) or large ones (inverse cascade). Athough these solutions have been tested in different systems, numerical and experimental works are currently a paramount of interest to understand in what extend this theory can describe real physical systems.

One of the most important system is Alfvén waves in magnetohydrodynamics (MHD) [6], initially observed in laboratory plasma [7–10], and recently in astrophysical plasma such as the Sun's outer [11] or inner [12] atmosphere. Three-dimensional (3D) Alfvén waves in a turbulent regime were initially predicted to follow the isotropic Iroshnikov-Kraichnan spectrum [13, 14]. However, they become strongly anisotropic in a presence of an intense magnetic field, and transfer energy mainly in the plane transverse to the field, thus becoming nearly two-dimensional [2, 15, 16]. The spectrum of this anisotropic weak turbulence regime has been derived [17, 18], then observed in the Jupiter's magnetosphere [19], and confirmed recently numerically [20, 21]. An analogous anisotropic behavior is predicted for hydrodynamics waves on the surface a magnetic fluid subjected to a horizontal magnetic field [22]. Although wave turbulence regimes have been observed on the surface of a ferrofluid in an external magnetic field both experimentally [23, 24] and numerically [25], the anisotropic regime has never been reported so far in such a system, to our knowledge.

In this Letter, we show the existence of an analogy between Alfvén wave turbulence and wave turbulence on the surface of a magnetic fluid. The analogy is not only qualitative but also quantitative in term of cascade of energy. In particular, we show that an anisotropic MHD wave turbulence emerges at high enough magnetic field with a wave spectrum showing similar scalings than the ones of anisotropic Alfvén wave turbulence predictions.

Theoretical backgrounds.— We consider an ideal incompressible magnetic liquid of infinite depth subjected to an external horizontal magnetic field B directed along the x-axis. The dispersion relation of linear waves on the surface of such a ferrofluid reads, neglecting gravity, [26]

$$\omega^2(\boldsymbol{k}) = [B^2/(\tilde{\mu}\rho)]k_x^2 + (\gamma/\rho)k^3 \ , \tag{1}$$

where $k \equiv |\boldsymbol{k}| = \sqrt{k_x^2 + k_y^2}$ is the wave number, ω is the angular frequency, γ and ρ are the surface tension and mass density of the liquid, $\tilde{\mu} = \mu_0(\mu+1)/(\mu-1)^2$, μ_0 is the magnetic permeability of vacuum, and μ is the relative permeability of the liquid. Equation (1) describes the anisotropic propagation of surface waves. We define $v_A^2 = B^2/(\tilde{\mu}\rho)$, the group velocity of dispersionless magnetic surface wave propagating along B (analogous to Alfvén velocity [6]). Note that μ is here constant, whereas μ experimentally depends of B [24]. This change has no impact here since v_A is the parameter used to quantify magnetic effects.

The power spectrum of wave elevation $S(k)$ is defined as the square modulus of the Fourier transform of the wave elevation $\eta(x, y)$. Without magnetic field, the KZ spectrum for isotropic capillary wave turbulence reads [4]

$$S^c(k) = C_{KZ} P^{1/2} (\gamma/\rho)^{-3/4} k^{-15/4} \ , \tag{2}$$

where C_{KZ} is the nondimensional KZ constant and P is the energy flux per unit area and density. The energy spectrum is $E^c(k) = (\gamma/\rho)k^2 S^c(k)$. To date, the KZ

* kochurin@iep.uran.ru
† eric.falcon@u-paris.fr

spectrum has been very well confirmed for capillary waves both experimentally (e.g., see [27–30]) and numerically [31–35] for weakly nonlinear capillary waves. For $B \neq 0$, no weak turbulence prediction for magneto-capillary waves exists so far, only dimensional analysis has been done [23, 24]. For Alfvén waves in a plasma within a strong magnetic field (e.g., along x), the energy transfer by three-wave interactions has been shown to be frozen in the field direction and to occur only in the transverse direction to B [15]. The weak turbulence predictions for the power spectrum of such anisotropic Alfvén wave turbulence ($k_y \gg k_x$, i.e., $|\boldsymbol{k}| \sim k_y$) reads [16–18]

$$S^m(k) = C_m P^{1/2} v_A^{-3/2} k_y^{-3}, \tag{3}$$

where $C_m = 1.467$ [36] (a $\sqrt{2\pi}$ factor was missing in [18]). The energy spectrum is $E^m(k) = v_a^2 k S^m(k)$.

Model equations.— The numerical model used here is based on the Hamiltonian equations describing the MHD motion of an ideal irrotational and incompressible ferrofluid subjected to an external horizontal magnetic field. We assume the absence of free electric charge and current in the fluid, which means that the magnetic field in the liquid is also potential. In the quadratic nonlinear approximation, the equations of boundary motion are written as

$$\eta_t = \hat{k}\psi - \hat{k}(\eta\hat{k}\psi) - \nabla_\perp(\eta\nabla_\perp\psi) + \hat{D}_k\eta \ , \tag{4}$$

$$\begin{aligned}\psi_t = {} & \nabla_\perp^2\eta + \frac{1}{2}\left[(\hat{k}\psi)^2 - (\nabla_\perp\psi)^2\right] + V_A^2\hat{k}^{-1}\eta_{xx} \\ & -\frac{A_\mu V_A^2}{2}\left[2\hat{k}^{-1}\partial_x\left(\eta\hat{k}\eta_x - \nabla_\perp\eta\cdot\nabla_\perp\hat{k}^{-1}\eta_x\right) - \eta_x^2\right. \\ & \left. -2\eta\eta_{xx} - (\nabla_\perp\hat{k}^{-1}\eta_x)^2\right] + \mathcal{F}(\boldsymbol{k},t) + \hat{D}_k\psi \ , \end{aligned} \tag{5}$$

where $\nabla_\perp = \{\partial_x, \partial_y\}$ is the nabla operator, ψ the velocity potential, $\hat{k}$ is the integral operator having the form $\hat{k}f_k = kf_k$, $\hat{k}^{-1}$ is the inverse $\hat{k}$-operator, $V_A^2 = v_A^2[\rho/(g\gamma)]^{1/2}$ is the nondimensional MHD wave speed, g is the gravity acceleration, and $A_\mu = (\mu-1)/(\mu+1)$ is the magnetic Atwood number. $\hat{D}_k$ is the viscosity operator acting as, $\hat{D}_k f_k = -\nu(k-k_d)^2 f_k$, for $k \geq k_d$, and, $\hat{D}_k = 0$, for $k < k_d$, the coefficient ν determines the intensity of energy dissipation (see [37–39]). More details on the derivation of Eqs. (4) and (5) from potential equations are given in the Supplemental Material [40]. The pumping term $\mathcal{F}(\boldsymbol{k},t)$ in Eq. (5) is defined in Fourier space as $\mathcal{F}(\boldsymbol{k},t) = F(k)\exp[i\omega(\boldsymbol{k})t]$, where $F(k) = F_0\exp[-(k-k_0)^4/k_f]$, with F_0 is the forcing amplitude reached at $k = k_0$. The wave vectors are pumped in the Fourier space in the range $k \in [1, k_f]$ (see below), and in all directions. In the absence of dissipation and pumping, exact analytical solutions of Eqs. (4)-(5) has been found in the strong-field limit and $\mu \gg 1$ [37, 38].

For finite μ, the surface waves collapse under the action of infinitely strong horizontal field [41]. Thus, for a correct simulation of the free surface MHD wave turbulence, it is necessary to take into account the regularizing effects of viscosity and surface tension.

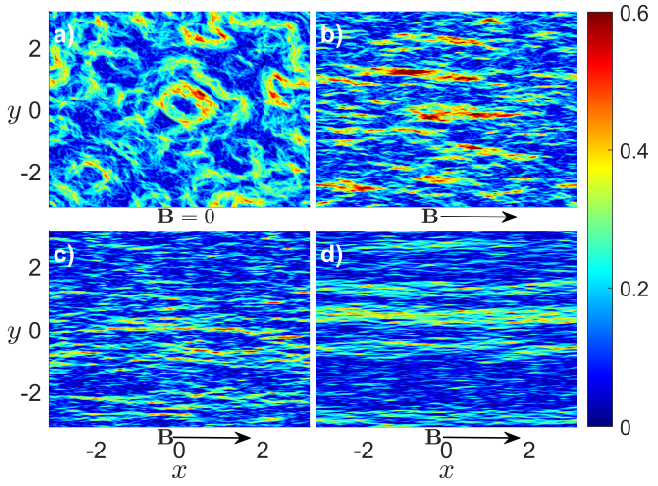

FIG. 1. Free surface gradient at a fixed time in the steady state ($t = 250$) for different values of B: $V_A^2 =$ (a) 0, (b) 25, (c) 100, and (d) 300. B is along the x-axis.

Equations (4) and (5) are solved numerically using the pseudo-spectral methods with the total number of Fourier harmonics $N \times N$. The time integration scheme is based on the explicit fourth-order Runge-Kutta method with a step dt. To stabilize the numerical scheme, a low-pass anti-aliasing filter is used [31]. At each integration time step, harmonics with wavenumbers greater than k_a are equated to zero. The effect of this low-pass filtering can be thus interpreted as "superviscosity" acting at small scales. Simulations are performed in a periodic box of size $2\pi \times 2\pi$ with $N = 1024$, $dt = 5 \times 10^{-5}$, $F_0 = 2000$, $k_0 = 3$, $k_f = 6$, $k_d = 150$, $k_a = 212$, and $\nu = 10$. All numerical simulations are carried out for a magnetic fluid with $A_\mu = 0.5$, which corresponds to $\mu = 3$. We present below four series of simulations with different values of the magnetic parameter $V_A^2 = 0$, 25, 100, and 300. The typical wave steepness $\epsilon \equiv \left\langle \sqrt{\int_{\mathcal{S}} ||\nabla\eta(x,y,t)||^2 dxdy/\mathcal{S}} \right\rangle_t$ used is 0.16 and is found to be almost constant when B is increased. The stationary state is reached after a time $t \approx 50$, and each simulation lasts up to $t = 500$.

Phenomenological analysis— The theoretical spectrum expected from our model equations [Eqs. (4) and (5)] is obtained following a phenomenological method described in Ref. [16, 36] and detailed in the Supplemental Material [40]. We assume a strong magnetic field ($V_A k_x \gg k_y^{3/2}$) and an anisotropy of the wave field ($k_y \gg k_x$). The fourth member of the rhs of Eq. (5) provides then an estimation of the nonlinear magnetic timescale as $T_{nl}^m \sim \psi/(V_A^2 k_x^2 \eta^2)$. Assuming that all the magnetic potential energy is transferred to capillary kinetic energy, one has $V_A^2 k_x \eta^2 \sim \psi^2 k_y$, and thus

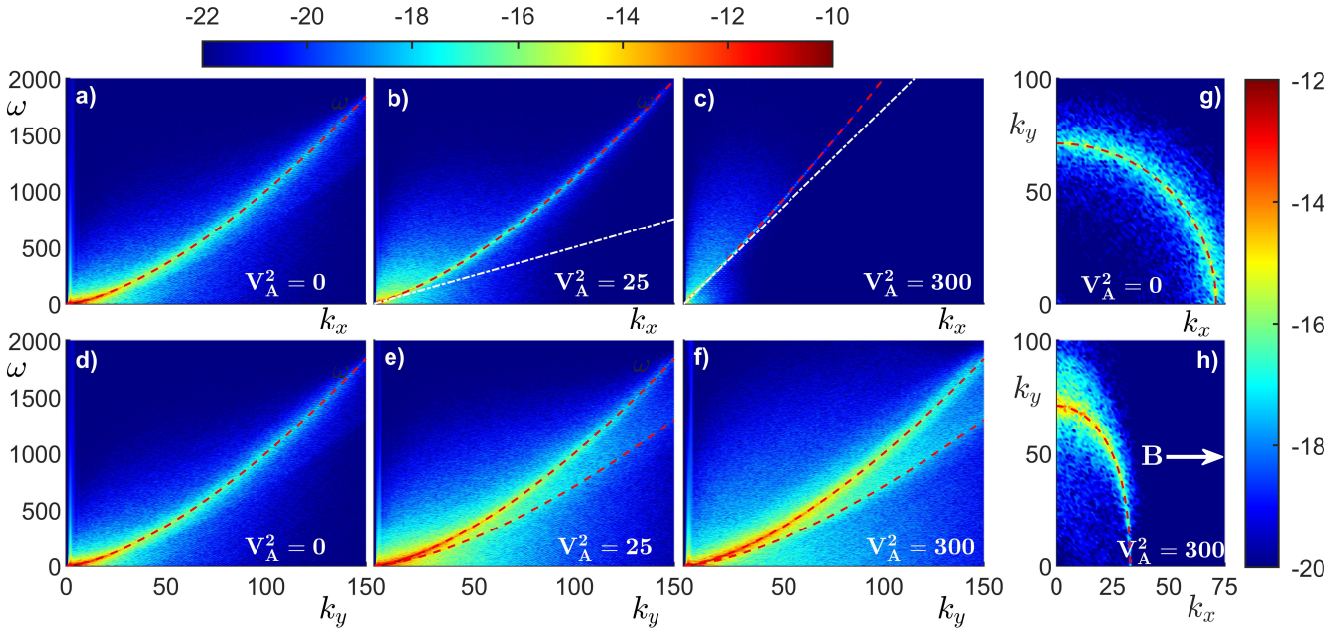

FIG. 2. (a)-(c) Power spectra $S(k_x, \omega)$ of surface waves in the field direction (x-axis) for different B, i.e., different V_A. Log-color bar. The red-dashed lines correspond to Eq. (1) (dispersion relation) and white dash-dotted lines to nondispersive wave propagation, $\omega = V_A k_x$. (d)-(f) Power spectra $S(k_y, \omega)$ of waves traveling along y-axis. The red dashed lines correspond to $\omega = k_y^{3/2}$ and $\omega = k_y^{3/2}/2^{1/2}$. (g) and (h): Cross sections $S(k_x, k_y, \omega^\star)$ of the power spectrum at a fixed frequency $\omega^\star = 600$ for different fields $V_A^2 = 0$ and $V_A^2 = 300$, respectively. Red-dashed lines correspond to $|\boldsymbol{k}(\omega^\star)|$ using Eq. (1).

$T_{nl}^m \sim 1/(\psi k_y k_x)$ with $\psi^2 \sim k_y E/k_x$. Using the power budget, the energy flux then reads $P \sim k_y E/(\omega T_{nl}^2)$, with E the energy spectrum. The power spectrum of wave elevations, $S^m(k) = E(k)/(V_A^2 k)$, finally reads $S^m(k) \sim P^{1/2} V_A^{-3/2} k_y^{-3}$, which is found to be the same as the shear-Alfvén wave turbulence prediction of Eq. (3).

Anisotropic regime.— Figure 1 shows the gradient of the free surface, at a fixed time in the steady state, for different B. We observe a transition from an isotropic regime [Fig. 1(a)] to a highly anisotropic regime [Fig. 1(d)]. Indeed, the surface relief in Fig. 1(d) becomes almost unidirectional, corresponding to surface waves propagating mainly in the direction perpendicular to B (see below). This anisotropy is due to the stabilizing effect of a horizontal magnetic field on a magnetic liquid. Indeed, for waves propagating in the field direction, the field lines pierce the wavy liquid-gas interface, and flatten it in the field direction as a consequence of the field boundary conditions at the interface [22, 42]. This behavior is close to the anisotropy observed when Alfvén waves propagate in the direction of a magnetic field [2], although of a different origin.

Nonlinear dispersion relation.— The anisotropy is also evidenced by the full power spectrum $S(k, \omega)$ of surface waves. Figures 2(a)-(c) show the spectrum $S(k_x, \omega)$ for waves traveling along the field direction for different B, i.e., different V_A. For $B = 0$, the energy injected at low k is redistributed within a large range of wave numbers around the linear dispersion relation of Eq. (1), as expected. When B is increased, the nonlinear dispersion relation is deformed [see Fig. 2(b)], then becomes quasi-dispersionless in the field direction [see Fig. 2(c)]. The spectra $S(k_y, \omega)$ of waves traveling normally to the field are shown in Figs. 2(d)-(f) for different B. Figure 2(d) corresponds to pure capillary waves ($B = 0$). When B is increased, waves of higher and higher wavenumbers are generated. Such enhanced energy transfers perpendicular to the field direction when the latter is increased, are a consequence of the anisotropic effect described above. Figures 2(e) and (f) display also the emergence of a second branch in the dispersion relation. This branch corresponds to bound waves (harmonics due to nonresonant interactions) [43]. Figures 2(g) and (h) show the cross sections $S(k_x, k_y, \omega^\star)$ of the power spectrum for a fixed frequency value, $\omega^\star$. For $B = 0$ [see Fig. 2(g)], the energy is distributed isotropically in all directions along a circle of radius $|\boldsymbol{k}(\omega^\star)|$ (only the first quadrant is shown). When B is increased, the energy is redistributed anisotropically, much stronger in the perpendicular direction than in the field direction [see Fig. 2(h)]. This effect is reported for all frequencies (see Supplemental Material [40]). A stronger nonlinear broadening also appears since bound waves occur normal to the field direction. To sum up, at high magnetic field, anisotropic wave propagation is observed ($k_y \gg k_x$) as expected by weak MHD (or shear-Alfvén) wave turbulence as well as appearance of nonlinear coherent structures in the y direction.

Wave interactions.— The MHD surface wave turbulence observed here involved nonlinear waves cascading

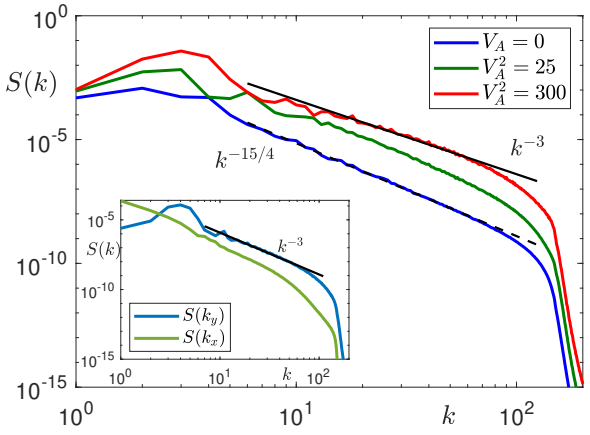

FIG. 3. Power spectra $S(k)$ of wave elevations for different V_A. Curves have been shifted for clarity. Dashed line: capillary-wave turbulence theory of Eq. (2) [4]. Solid line: anisotropic MHD wave turbulence theory of Eq. (3). Inset: Spectra in the field direction $S(k_x)$ (green line) and normal to the field $S(k_y)$ (blue line). $V_A^2 = 300$.

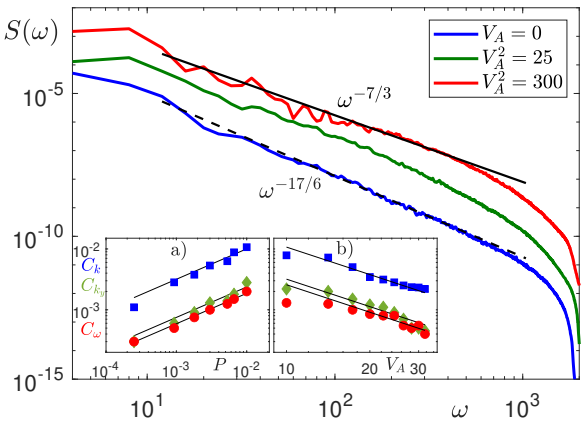

FIG. 4. Power spectra $S(\omega)$ of wave elevations for different V_A. Curves have been shifted for clarity. Dashed line: capillary-wave turbulence theory in $\omega^{-17/6}$ from Eq. (2) using $\omega \sim k^{-3/2}$ [4]. Solid line: predictions for anisotropic MHD surface wave turbulence from Eq. (3) with $\omega \sim k^{-3/2}$. Inset: spectrum coefficients C_k (square), C_{k_y} (diamond) and C_ω (circle) versus (a) P for fixed $V_A^2 = 300$, and (b) V_A for fixed $P \approx 2.7 \times 10^{-3}$. Solid lines: best fits in $P^{1/2} V_A^{-3/2}$.

towards small scales as a result of anisotropic three-wave resonant interactions occurring mainly in the perpendicular direction of the magnetic field (see inset of Fig. 3). These three-wave resonant interactions are well evidenced by computing the third-order correlation (or bicoherence) of wave elevations (see Supp. Mat. [40]).

Wave-number spectrum.— To quantify the transition from isotropic capillary wave turbulence to anisotropic MHD wave turbulence, we compute the power spectra of surface elevations in frequency, $S(\omega)$ and in wave number $S(k)$. $S(k)$ is shown in Fig. 3 for different V_A. At zero field, the spectrum is in good agreement with the KZ spectrum in $k^{-15/4}$ of Eq. (2). At intermediate field, the spectrum exponent decreases slightly, but is still close to the one predicted by weak turbulence theory. At high enough field, we observe a transition from the KZ spectrum to a spectrum in k^{-3} in rough agreement with the scaling of the phenomenological model and of anisotropic Alfvén wave turbulence of Eq. (3) (see main Fig. 3). Specifically, the inset of Fig. 3 shows the spectra $S(k_x)$ along the field direction (x-axis) and $S(k_y)$ perpendicular to it (y-axis) for $V_A^2 = 300$. $S(k_y)$ is found to scale as k_y^{-3} as expected by Eq. (3) whereas $S(k_x)$ is more than one order of magnitude smaller than $S(k_y)$ in the inertial range. Thus, the spectrum, $S(k) = C_k(P, V_A)k^{-3}$, observed in the main Fig. 3, is mainly due to the energy transferred perpendicularly to the external field. We determine now the scaling of the coefficient C_k with the energy flux P and with the magnetic parameter V_A by performing two series of simulations: (i) at a fixed magnetic field ($V_A^2 = 300$) for different amplitudes of the energy pumping; (ii) at a fixed rate of energy dissipation P for different fields. The spectrum is then found to increase with the pumping as $C_k(P) \sim P^{1/2}$ [see inset (a) of Fig. 4] and to decrease with the magnetic field as $C_k \sim V_A^{-3/2}$ [see inset (b)] for high enough V_A. Note that C_{k_y}, the coefficient of the spectrum $S(k_y)$, is observed to follow the same scaling. When returning to the dimensional variables, we find thus

$$S(k) \approx S(k_y) = C P^{1/2} v_A^{-3/2} k_y^{-3} \ , \qquad (6)$$

where C is a constant, independent of P and V_A, to be found numerically (see below). Equation (6) is similar to the spectrum scalings found above by the phenomenological model and to Eq. (3) describing anisotropic Alfvén waves in plasma subjected to a strong magnetic field. Although MHD surface waves on a magnetic fluid is physically different from MHD Alfvén waves in plasma, the anisotropic effect on the energy transfer due to the magnetic field is common and leads to the same scaling for the wave spectrum. Note that, in plasma, no wave propagates normal to the field (only magnetic energy is transferred to the normal direction by shearing) whereas, in our case, capillary waves propagates normal to the field, the magnetic energy being transferred to capillary energy.

Frequency spectrum.— We compute now the frequency spectrum $S(\omega)$ for different V_A as shown in Fig. 4. At zero field, the simulations again show a good agreement with the predicted KZ spectrum in $S(\omega) \sim \omega^{-17/6}$ [4]. At large enough B, the spectrum is less steep and scales as $S(\omega) = C_\omega \omega^{-7/3}$. The coefficient C_ω is found to scale as $P^{1/2}$ and $V_A^{-3/2}$ (see insets of Fig. 4) as for C_k. Returning to the dimensional variables thus leads to

$$S(\omega) = C'(\gamma/\rho)^{2/3} P^{1/2} v_A^{-3/2} \omega^{-7/3} \ . \qquad (7)$$

where C' is a constant. Note that the empirical spectra of Eqs. (6)-(7) are found to be consistent with each

other since they verify $S(\omega)d\omega = S(k)dk \approx S(k_y)dk_y$, using $k_y \gg k_x$ and $\omega(k)$ from Eq. (1). This also gives $C' = 2C/3$. We find the values of the constants $C = 1.7$ and $C' = 1.34$ (using the best fits of C_{k_y} and C_ω in Fig. 4a). C is close to the theoretical value $C_m = 1.467$ found for shear-Alfvén wave turbulence in plasma [36] and the ratio $2C/3C' = 0.85$ is as expected close to 1. Moreover, the spectrum scaling with the energy flux in $P^{1/2}$ is consistent with the fact that three-wave resonant interactions are involved here [2]. Finally, the timescale separation hypothesis of wave turbulence is verified here since the nonlinear time is found much longer than the linear time regardless of k (see Supplemental Material [40]). A typical resonant triad is also shown in [40] to highlight that resonant wave vectors are of the same order of magnitude suggesting that wave interactions are local. Our results thus differ from two-dimensional MHD weak-turbulence predictions leading to nonlocal interactions and a flat steady-state spectrum [44].

Conclusion.— We have numerically reported a transition from isotropic capillary-wave turbulence to a strongly anisotropic MHD wave turbulence on a surface of a magnetic fluid, for high enough magnetic field. In this anisotropic regime, the wave spectrum is found to be in good agreement with the prediction of three-dimensional weak MHD (shear-Alfvén) wave turbulence. This highlights the broad application of weak wave turbulence where different physical systems can lead to similar phenomena, only because they share similar dispersion relations and the same nonlinear interaction process (three-wave resonant interactions). Such quantitative analogy between Alfvén waves in plasma and surface waves on magnetic fluids would deserve further studies in particular theoretically, and could lead to a better understanding of plasma by studying them more easily. The analogy discovered here could be pushed forward to explore open questions in wave turbulence such as the properties of large scales [30], or the critical balance separating weak turbulence from strong turbulence [21]. The phenomenon reported here could also be observed experimentally using a ferrofluid with a high magnetic susceptibility and a high saturation magnetization. However, such ferrofluids are currently still too viscous (at least ten times the water value) which would prevent wave interactions to occur. Finally, similar effects should be expected in electrohydrodynamics of nonconducting liquids in a strong electric field due to the equivalence between the underlying equations [45].

ACKNOWLEDGMENTS

E. Kochurin's work on developing the numerical tools is supported by Russian Science Foundation, project No. 21-71-00006. E. Falcon thanks partial support of the French National Research Agency (ANR DYSTURB project No. ANR-17-CE30-0004), and of the Simons Foundation MPS N°651463-Wave Turbulence.

[1] V. E. Zakharov, G. Falkovitch, and V. S. L'vov, *Kolmogorov Spectra of Turbulence I: Wave Turbulence* (Springer-Verlag, Berlin, 1992).
[2] S. Nazarenko, *Wave turbulence* (Springer-Verlag, Berlin, 2011).
[3] V. E. Zakharov, Energy spectrum for stochastic oscillations of the surface of a liquid, Sov. Phys. Dokl. **11**, 881 (1967).
[4] V. E. Zakharov, and N. N. Filonenko, Weak turbulence of capillary waves, J. Appl. Mech. Tech. Phys. **8**, 37 (1967).
[5] V. E. Zakharov, and R. Z. Sagdeev, Spectrum of acoustic turbulence, Dokl. Akad. Nauk. **192**, 297 (1970).
[6] H. Alfvén, Existence of Electromagnetic-Hydrodynamic Waves, Nature, **150**, 405 (1942)
[7] S. Lundquist, Experimental Investigations of Magneto-Hydrodynamic Waves, Phys. Rev. **76**, 1805 (1949)
[8] W. H. Bostick and M. A. Levine, Experimental Demonstration in the Laboratory of the Existence of Magneto-Hydrodynamic Waves in Ionized Helium, Phys. Rev. **87**, 671 (1952)
[9] B. Lehnert, Magneto-Hydrodynamic Waves in Liquid Sodium, Phys. Rev. **94**, 815 (1954)
[10] T. K. Allen, W. R. Baker, R. V. Pyle, and J. M. Wilcox, Experimental Generation of Plasma Alfven Waves, Phys. Rev. Lett. **2**, 383 (1959)
[11] B. De Pontieu, Chromospheric Alfvénic Waves Strong Enough to Power the Solar Wind, Science **318**, 1574 (2007)
[12] J. C. Kasper, K. G. Klein, E. Lichko, J. Huang, C. H. K. Chen, S. T. Badman *et al.*, Parker Solar Probe Enters the Magnetically Dominated Solar Corona, Phys. Rev. Lett. **127**, 255101 (2021)
[13] P. Iroshnikov, Turbulence of a Conducting Fluid in a Strong Magnetic Field, Soviet Astron. **7**, 566 (1964)
[14] R. H. Kraichnan, Inertial-Range Spectrum of Hydromagnetic Turbulence, Phys. Fluids **8**, 1385 (1965)
[15] J. V. Shebalin, W. H. Matthaeus, and D. Montgomery, Anisotropy in MHD turbulence due to a mean magnetic field, J. Plasma Phys. **29**, 525 (1983)
[16] S. Galtier, *Introduction to Modern Magnetohydrodynamics* (Cambridge University Press, Cambridge, 2016); S. Galtier, Turbulence in space plasmas and beyond, J. Phys. A: Math. Theor. **51**, 293001 (2018).
[17] C. S. Ng, and A. Bhattacharjee, Scaling of anisotropic spectra due to the weak interaction of shear-Alfvén wave packets, Phys. Plasmas **4**, 605 (1997)
[18] S. Galtier, S. Nazarenko, A. Newell, and A. Pouquet, A weak turbulence theory for incompressible magnetohydrodynamics, J. Plasma Phys., **63**, 447 (2000)
[19] J. Saur, H. Politano, A. Pouquet, and W. H. Matthaeus, Evidence for weak MHD turbulence in the middle magnetosphere of Jupiter, Astron. Astrophys. **386**, 699 (2002)

[20] R. Meyrand, K. Kiyani, and S. Galtier, Weak magnetohydrodynamic turbulence and intermittency, J. Fluid Mech. **770**, R1 (2015)

[21] R. Meyrand, S. Galtier, and K. H. Kiyani, Direct evidence of the transition from weak to strong magnetohydrodynamic turbulence, Phys. Rev. Lett. **116**, 105002 (2016)

[22] R. E. Rosensweig, *Ferrohydrodynamics*, (Dover Publications, New York, 1997)

[23] F. Boyer and E. Falcon, Wave Turbulence on the Surface of a Ferrofluid in a Magnetic Field, Phys. Rev. Lett. **101**, 244502 (2008).

[24] S. Dorbolo and E. Falcon, Wave turbulence on the surface of a ferrofluid in a horizontal magnetic field, Phys. Rev. E **83**, 046303 (2011).

[25] E. A. Kochurin, Numerical simulation of the wave turbulence on the surface of a ferrofluid in a horizontal magnetic field, J. Magn. Magn. Mater. **503**, 166607 (2020).

[26] J. R. Melcher, Electrohydrodynamic and magnetohydrodynamic surface waves and instabilities, Phys. Fluids **4**, 1348 (1961).

[27] E. Falcon, C. Laroche, and S. Fauve, Observation of Gravity-Capillary Wave Turbulence, Phys. Rev. Lett. **98**, 094503, (2007).

[28] C. Falcón, E. Falcon, U. Bortolozzo, and S. Fauve, Capillary wave turbulence on a spherical fluid surface in low gravity, Europhys. Lett. **86**, 14002 (2009).

[29] G. V. Kolmakov, M. Y. Brazhnikov, A. A. Levchenko, L. V. Abdurakhimov, P. V. E. McClintock, and L. P. Mezhov-Deglin, Capillary Turbulence on the Surfaces of Quantum Fluids, Prog. Low Temp. Phys. **16**, 305 (2009).

[30] E. Falcon and N. Mordant, Experiments in Surface Gravity–Capillary Wave Turbulence, Annu. Rev. Fluid Mech. **54**, 1 (2022).

[31] A. N. Pushkarev and V. E. Zakharov, Turbulence of Capillary Waves, Phys. Rev. Lett. **76**, 3320 (1996).

[32] A. N. Pushkarev and V. E. Zakharov, Turbulence of capillary waves: theory and numerical simulation, Physica (Amsterdam) **135D**, 98 (2000).

[33] L. Deike, D. Fuster, M. Berhanu, and E. Falcon, Direct Numerical Simulations of Capillary Wave Turbulence, Phys. Rev. Lett. **112**, 234501 (2014).

[34] Y. Pan and D. K. P. Yue, Direct Numerical Investigation of Turbulence of Capillary Waves, Phys. Rev. Lett. **113**, 094501 (2014).

[35] Y. Pan and D. K. P. Yue, Decaying capillary wave turbulence under broad-scale dissipation, J. Fluid Mech. **780**, R1 (2015).

[36] S. Galtier, *Physique de la turbulence* (EDP Sciences/ CNRS Editions, Paris 2021), Ch. 9, pp. 223–248

[37] N. M. Zubarev, Nonlinear waves on the surface of a dielectric liquid in a strong tangential electric field, Phys. Lett. A **333**, 284 (2004).

[38] N. M. Zubarev, Nonlinear waves on the surface of a dielectric liquid in a horizontal electric field in 3D geometry: exact solutions, JETP Lett. **89**, 271 (2009).

[39] N. M. Zubarev and E. A. Kochurin, Three-dimensional nonlinear waves at the interface between dielectric fluid in an external horizontal electric field, J. Appl. Mech. Tech. Phys. **54**, 212 (2013).

[40] See Supplemental Material at http://link.aps.org/... for additional information on: (i) details of the numerical model, (ii) stationarity of the total energy and probability distribution of the wave field, (iii) wave field images, (iv) effects of anisotropy on the wave spectrum and on the correlations of the wave elevations, (v) verification of timescale separation, and (vi) derivation of the phenomenological model of the wave spectrum and nonlinear timescales.

[41] E. A. Kochurin, O. V. Zubareva, and N. M. Zubarev, Wave breaking on the surface of a dielectric liquid in a horizontal electric field, IEEE Tran. Diel. Elec. Ins. **27**, 1222 (2020).

[42] C. A. Walsh, Magnetized ablative Rayleigh-Taylor instability in three dimensions, Phys. Rev. E **105**, 025206 (2022).

[43] E. Herbert, N. Mordant, and E. Falcon, Observation of the Nonlinear Dispersion Relation and Spatial Statistics of Wave Turbulence on the Surface of a Fluid, Phys. Rev. Lett. **105**, 144502 (2010)

[44] N. Tronko, S. V. Nazarenko, and S. Galtier, Weak turbulence in two-dimensional magnetohydrodynamics, Phys. Rev. **87**, 033103 (2013).

[45] E. A. Kochurin, Wave Turbulence of a Liquid Surface in an External Tangential Electric Field, JETP Lett. **109**, 303 (2019).

Supplemental Material of "Three-dimensional direct numerical simulation of free-surface magnetohydrodynamic wave turbulence"

Evgeny Kochurin,[1,2] Guillaume Ricard,[3] Nikolay Zubarev,[2,4] and Eric Falcon[3]

[1] *Skolkovo Institute of Science and Technology, 121205, Moscow, Russia*
[2] *Institute of Electrophysics, Ural Division, Russian Academy of Sciences, Yekaterinburg, 620016 Russia*
[3] *Université Paris Cité, CNRS, MSC Laboratory, UMR 7057, F-75 013 Paris, France*
[4] *Lebedev Physical Institute, Russian Academy of Sciences, Moscow, 119991 Russia*

In this Supplemental Material, we present additional data analyses related to wave turbulence on the surface of a magnetic fluid subjected to a horizontal magnetic field: details of the numerical model (Sec. I), stationarity of the total energy and probability distribution of the wave field (Sec. II), wave field images (Sec. III), effects of anisotropy on the wave spectrum and on the correlations of the wave elevations (Sec. IV), verification of the timescale separation (Sec. V), and derivation of the phenomenological model of the wave spectrum and nonlinear timescales (Sec. VI). Notations as in the aforementioned text.

I. NUMERICAL MODEL

We consider a potential flow of an ideal incompressible ferrofluid. The velocity potential $\Phi(\mathbf{r})$ satisfies the Laplace equation $\Delta\Phi = 0$, at $z < \eta$. Maxwell's equations are reduced to a static boundary value problem at each moment in time: magnetic field lines instantly adjust to the curved fluid boundary. This approximation is valid if the typical velocity of the liquid surface is much less than the speed of light. Such a condition is thus fully fulfilled. We suppose that the magnetic fluid is dielectric (there are no free electric current), i.e., the magnetic field strength $H_{1,2}(\mathbf{r})$ is characterized by magnetic scalar potentials $H_{1,2} = -\nabla\varphi_{1,2}$, where the indices "1" and "2" correspond to the regions inside the liquid and above its free boundary, respectively. The magnetic potentials obey the Laplace equation $\Delta\varphi_{1,2} = 0$, at $z \neq \eta$. The boundary conditions for Maxwell's equations in terms of the magnetic potential are written as $\varphi_1 = \varphi_2$ and $\mu\partial_n\varphi_1 = \partial_n\varphi_2$ at $z = \eta(x, y, t)$, and $\varphi_{1,2} = -(B/\mu_0)x$ at $z = \mp\infty$, where ∂_n is normal derivative to the free surface, and B is the external magnetic field induction. The evolution of the system is described by kinematic and dynamic boundary conditions at $z = \eta(x, y, t)$ as

$$\eta_t = \Phi_z - \nabla_\perp\eta\cdot\nabla_\perp\Phi, \qquad \Phi_t + \frac{(\nabla\Phi)^2}{2} - \sigma\nabla_\perp\cdot\frac{\nabla_\perp\eta}{\sqrt{1+(\nabla_\perp\eta)^2}} = \frac{\mu_0(\mu-1)}{2\rho}\left(\nabla\varphi_1\cdot\nabla\varphi_2 - \frac{B^2}{\mu_0^2}\right). \tag{s1}$$

The above equations are a closed system describing the fully nonlinear evolution of a magnetic fluid with free surface taking into accounts the effects of capillary and magnetic forces. The total energy of the system (Hamiltonian) has the following form

$$\mathcal{H} = \frac{1}{2}\int\limits_{z\le\eta}(\nabla\Phi)^2 d\mathbf{r} - \frac{\mu_0\mu}{2}\int\limits_{z\le\eta}(\nabla\varphi_1)^2 - (B/\mu_0)^2 d\mathbf{r} - \frac{\mu_0}{2}\int\limits_{z\ge\eta}(\nabla\varphi_2)^2 - (B/\mu_0)^2 d\mathbf{r} + \int\frac{\sigma}{\rho}\left(\sqrt{1+\nabla_\perp\eta}-1\right)dxdy.$$

The equations of boundary motion (s1) can be obtained using the variational derivatives

$$\frac{\partial\eta}{\partial t} = \frac{\delta\mathcal{H}}{\delta\psi}, \qquad \frac{\partial\psi}{\partial t} = -\frac{\delta\mathcal{H}}{\delta\eta}, \tag{s2}$$

the quantities $\eta(x, y, t)$ and $\psi(x, y, t) = \Phi(x, y, z = \eta, t)$ play the role of canonical variables. The procedure for obtaining weakly nonlinear equations is well described in the works [1-4, 37-39]. The model used is based on the quadratically nonlinear equation system initially formulated in the framework of Hamiltonian formalism for the description of electrohydrodynamic motion of dielectric liquids in [37-39] (the problem is mathematically completely equivalent to the current study).

We use nondimensional units, i.e., $\tilde{t} = t/t_0$ and $\tilde{r} = r/\lambda_0$, with $t_0 = 2\pi[\gamma/(\rho g^3)]^{1/4}$ and $\lambda_0 = 2\pi[\gamma/(\rho g)]^{1/2}$ (the

tilde notation is omitted hereafter for the sake of clarity). The Hamiltonian is expressed in the following form [37]

$$\mathcal{H} = \frac{1}{2}\iint \Big[(\nabla_\perp \eta)^2 + \psi \hat{k}\psi - \eta\left((\hat{k}\psi)^2 - (\nabla_\perp \psi)^2\right) + V_A^2\left(\eta_x \hat{k}^{-1}\eta_x + A_\mu\left[\eta\eta_x^2 - \eta_x\hat{k}^{-1}\eta\hat{k}\eta_x + \eta_x\hat{k}^{-1}(\nabla_\perp\eta\cdot\nabla_\perp\hat{k}^{-1}\eta_x)\right]\right)\Big]\, dxdy. \quad \text{(s3)}$$

Taking the variational derivatives from Eq. (s3) and adding to the Eq. (s2) terms responsible for the effects of pumping and dissipation of energy, we get the governing Eqs. (4)-(5) of the main text.

II. TOTAL ENERGY AND WAVE PROBABILITY DISTRIBUTIONS

The total energy of the system is shown in Fig. S1 as a function of time for different magnetic fields. It shows that the system reaches a quasi-stationary state from $t \approx 50$. The probability density functions (PDF) of the rescaled wave elevations in this stationary regime are shown in the inset for different magnetic fields. The PDF asymmetry is weak (skewness $S = \langle\eta^3\rangle/\langle\eta^2\rangle^{3/2} < 0.02$) regardless of the field value. Its flatness (kurtosis $K = \langle\eta^4\rangle/\langle\eta^2\rangle^2$) is found to decrease with an increasing magnetic field: close to 3 (Gaussian) for weak B down to 2.45 at the maximum field. The PDF departs from Gaussian and becomes narrower with increasing magnetic field.

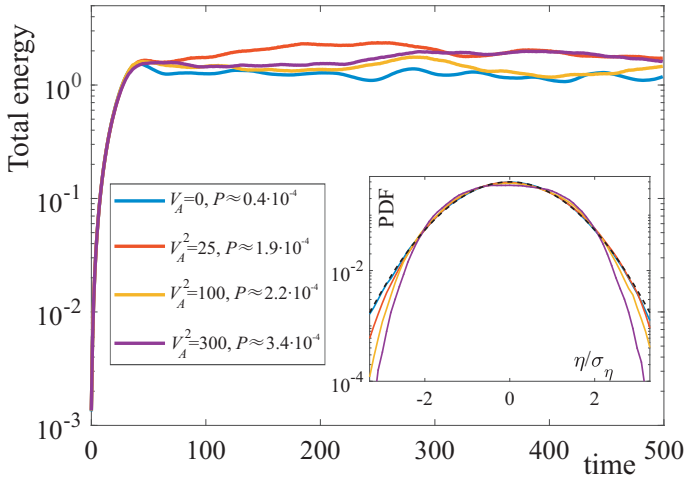

Figure S1: Total energy of the system versus time for the different values of the magnetic parameter V_A and of the resulting energy dissipation fluxes, P, for each series of simulations. Inset: PDF of the wave elevations rescaled by the standard deviation η/σ_η (colored dots). Black-dashed line corresponds to a Gaussian fit.

III. FREE SURFACE ELEVATION

The free-surface elevation in the stationary regime is shown in Fig. S2 for different magnetic fields and evidence similar results on the anisotropy effects discussed in the main text.

IV. ANISOTROPY

The anisotropy is observed in the cross sections of the spectrum of wave elevations, $S(k_x, k_y, \omega^\star)$, for fixed $\omega^\star$ [see Fig. 2 (g)-(h) of the main text for $\omega^\star = 600$]. This anisotropy is valid regardless of ω^* as shown in Fig. S3(a)-(d).

Anisotropy is also observable looking at the three-wave resonant interactions which read

$$\omega(k_1) + \omega(k_2) - \omega(k_1 + k_2) = 0\,. \quad \text{(s4)}$$

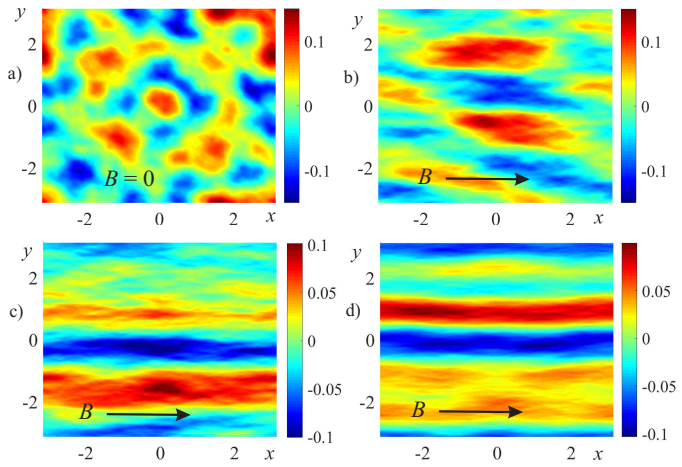

Figure S2: The free-surface elevations at $t = 250$ in the stationary regime for different values of the magnetic parameter: (a)-(d) correspond to $V_A^2 = 0$, 25, 100, and 300, respectively.

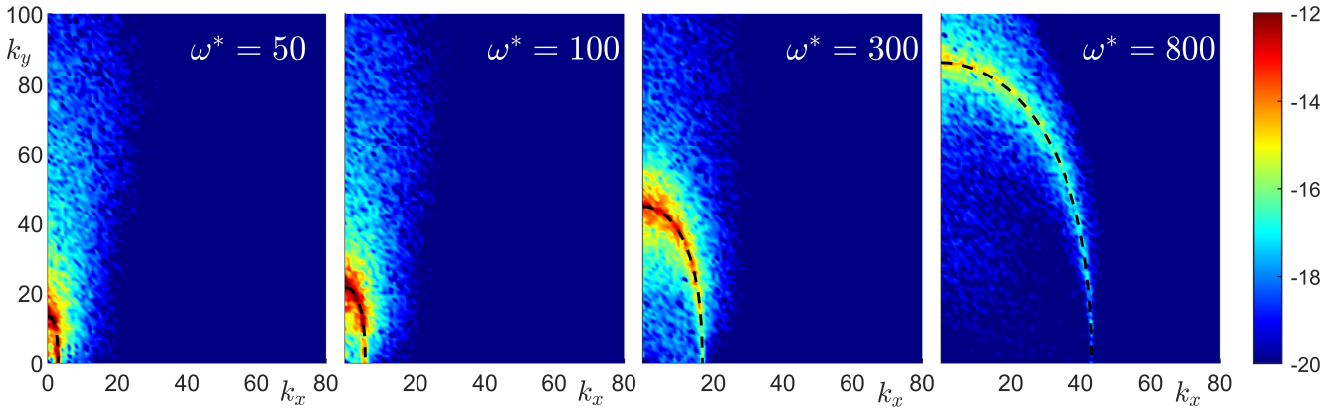

Figure S3: Cross sections $S(k_x, k_y, \omega^\star)$ of the power spectrum for a fixed frequency $\omega^\star$ = (a) 50, (b) 100, (c) 300, and (d) 800, for $V_A^2 = 300$. Black-dashed lines correspond to $|k(\omega^\star)|$. Only the first quadrant is plotted. Log colorbar.

with $\omega(k)$ the dispersion relation of Eq. (1). Such three-wave resonant interactions are quantified by computing the normalized third-order correlations in k of wave elevations (called bicoherence) as

$$B(k_1, k_2) = \frac{|\langle \eta_{k_1} \eta_{k_2} \eta^*_{k_1+k_2} \rangle|}{\sqrt{\langle |\eta_{k_1} \eta_{k_2}|^2 \rangle \langle |\eta_{k_1+k_2}|^2 \rangle}}\,. \tag{s5}$$

where $*$ denotes the complex conjugate, the normalization being chosen to bound B between 0 (no correlation) and 1 (perfect correlation). $B[k_1, k_2(k_x, k_y)]$ is plotted in Fig. S4 for a fixed k_1, at different magnetic fields. The triad of interactions are closer to $k_x = 0$ at high magnetic field, which evidences again the anisotropic effects.

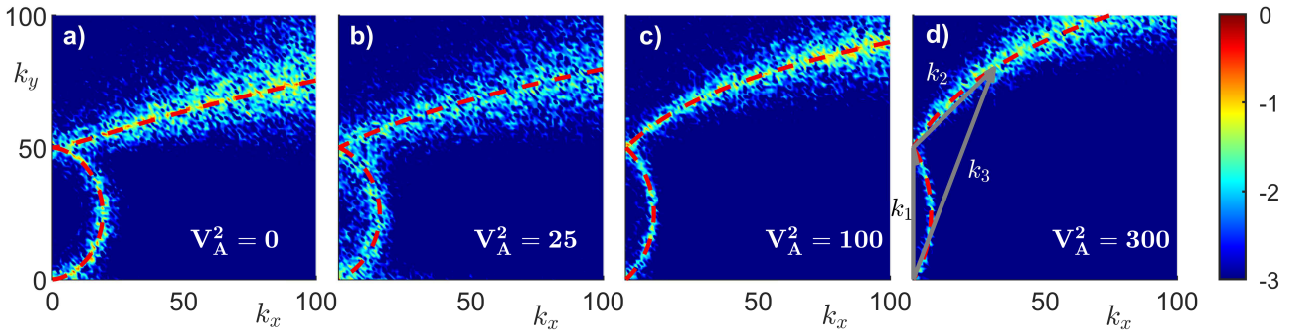

Figure S4: Bicoherences $B[k_1, k_2(k_x, k_y)]$ for a given wave vector $k_1 = (k_x = 0, k_y = 50)$, and different V_a^2 = (a) 0, (b) 25, (c) 100, and (d) 300. Dashed lines: theoretical solutions obtained solving Eq. (s4) for fixed $k_1 = (0, 50)$ using Eq. (1). A resonant triad $[k_1(0, 50)$, $k_2(30.68, 30)$, $k_3(-30.68, -80)]$ is displayed in (d) with wave vectors of same order of magnitude ($|k_1| = 50$, $|k_2| = 43$, $|k_3| = 86$) as expected for local interactions. Log colorbar.

V. TIMESCALES OF WAVE TURBULENCE

Weak turbulence theory assumes a scale separation which can be evaluated using timescales [30] as

$$\tau_l(k) \ll \tau_{nl}(k), \tag{s6}$$

where τ_l is the linear timescale and τ_{nl} the nonlinear timescale. Equation (s6) requires that nonlinear interactions are much slower than fast linear oscillations of the waves, to let the energy cascade of wave turbulence to occur. $\tau_l(k)$ is directly linked to the dispersion relation as $\tau_l(k) = 1/\omega(k)$ whereas $\tau_{nl}(k)$ is estimated using the spectrum broadening of Fig. (2). This broadening $\delta_\omega(k)$ is estimated, for each k, by fitting the corresponding spectrum $S_\eta(k, \omega)$ by a Gaussian function of ω, the standard deviation of this fit gives δ_ω. This broadening being due to nonlinear effects, τ_{nl} is usually estimated as $\tau_{nl} = 1/\delta_\omega$ [30]. The timescales found are then plotted in Fig. S5 as a function of k_y, i.e., in the direction perpendicular to the field. Figure S5 hence shows that Eq. (s6) is well verified over the inertial range where wave turbulence is observed (see Fig. 3), and regardless of the magnetic field value. The critical balance (i.e., $\tau_l \sim \tau_{nl}$) is not achieved here [2,16,21,36].

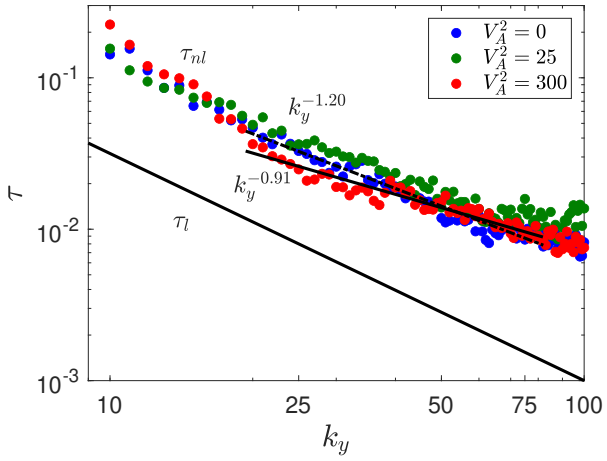

Figure S5: Linear and nonlinear timescales, (−) τ_l and (•) τ_{nl}, versus k_y for three values of the magnetic field. Solid line: best fit in $k_y^{-0.91\pm0.1}$ for $V_A^2 = 300$ and high k_y. Dashed line: best fit in $k_y^{-1.20\pm0.2}$ for $V_A^2 = 0$ and high k_y.

VI. PHENOMENOLOGICAL DERIVATIONS OF THE SPECTRUM AND NONLINEAR TIMESCALE

Using the phenomenology method described in Refs. [16,36], we obtain below the theoretical expressions of the energy spectrum and magnetic nonlinear timescale.

A. Energy spectrum

Let us assumed a strong magnetic field ($V_A k_x \gg k_y^{3/2}$) and anisotropy ($k_y \gg k_x$). From Eq. (5), we get

$$T_{nl}^c \sim \frac{1}{\psi k_y^2} \quad \text{and} \quad T_{nl}^m \sim \frac{\psi}{V_A^2 k_x^2 \eta^2} \tag{s7}$$

where T_{nl}^c and T_{nl}^m are the capillary and magnetic nonlinear times obtained from the equation of motion of Eq. (5), and ψ the velocity potential. We assume now that the magnetic nonlinear effects dominate and that an energy equipartition exists between the magnetic potential energy and the capillary kinetic energy. Magnetic kinetic energy is negligible since no wave travels in the x direction and the potential surface energy is supposed to be dominated by magnetic effects. This leads to

$$V_A^2 k_x \eta^2 \sim \psi^2 k_y, \tag{s8}$$

and thus inserting Eq. (s8) into Eq. (s7) gives

$$T_{nl}^m \sim \frac{1}{\psi k_y k_x}. \tag{s9}$$

Using the power budget, the energy flux P reads

$$P \sim \frac{k_x k_y E^{(2D)}}{\tau_{nl}}, \tag{s10}$$

with τ_{nl} the nonlinear time involved in the kinetic equation (also called the transfer time of the energy flux in Refs. [16,36]). T_{nl} and τ_{nl} are linked by $\tau_{nl} \sim \omega T_{nl}^2$ since for three-wave interactions [2]. Using $\psi^2 \sim k E^{(2D)}$ leads to the two-dimensional (2D) energy spectrum:

$$E^{(2D)} \sim P^{1/2} V_A^{1/2} k_y^{-2} k_x^{-1}. \tag{s11}$$

The scaling in k_x being irrelevant in anisotropic system and after an integration over k_x, i.e., $E^{(1D)} \sim k_x E^{(2D)}$, we get the unidimensional (1D) energy spectrum

$$E^{(1D)} \sim P^{1/2} V_A^{1/2} k_y^{-2}, \tag{s12}$$

Finally, using the relationship $E^{(1D)}(k) = V_A^2 k S^m(k)$ between the magnetic energy spectrum, $E^{(1D)}(k)$, and the power spectrum of wave elevation, $S^m(k)$, and $k = \sqrt{k_x^2 + k_y^2} \simeq k_y$ (since $k_y \gg k_x$), we obtain phenomenologically,

$$S^m(k) \sim P^{1/2} V_A^{-3/2} k_y^{-3}, \tag{s13}$$

in agreement with the spectra observed numerically [see Eq. (6)] and derived theoretically [see Eq. (3)] for anisotropic Alfvén wave turbulence [16-18]. The strong hypotheses used above are not fully true numerically for every k, and could explain the reduced inertial range where this spectrum is numerically observed.

B. Magnetic nonlinear timescale

From Eq. (s9), $\psi^2 \sim k_y E^{(2D)}$, and Eq. (s11), we get the full scaling of the magnetic nonlinear time of the equations of motion as

$$T_{nl}^m \sim P^{-1/4} V_A^{-1/4} k_x^{-1/2} k_y^{-1/2}, \tag{s14}$$

and of the magnetic nonlinear time of the kinetic wave equation as

$$\tau_{nl}^{m} \sim P^{-1/2} V_A^{1/2} k_y^{-1}. \tag{s15}$$

Figure S5 shows that the magnetic nonlinear timescale found numerically for strong magnetic field ($V_A^2 = 300$) scales as $\tau_{nl} \sim k_y^{-0.93\pm0.1}$ for high k_y, and is thus very close to the expected scaling in k_y^{-1} of Eq. (s15).

For pure capillary waves ($V_A^2 = 0$), a similar phenomenology leads to $\tau_{nl}^{c} \sim P^{-1/2}(\gamma/\rho)^{1/4} k^{-3/4}$ [36]. Note that τ_{nl}^{c} could be obtained using dimensional analysis [30]. Figure S5 shows that the capillary nonlinear time found numerically for zero magnetic field ($V_A^2 = 0$) scales as $\tau_{nl} \sim k_y^{-1.25\pm0.2}$ for high k_y, which departs from the $k^{-3/4}$ prediction.

C. Timescale separation

Wave turbulence is expected to occur if the timescale separation hypothesis, $\tau_l(k) \ll \tau_{nl}(k)$, is verified. Using Eq. (s15) and the numerical values obtained for $V_A^2 = 300$ [i.e., $P = 2.7 \times 10^{-3}$ and the most probable values of $(k_x, k_y) = (14, 65)$ inferred from Fig. 2(h)], we indeed obtain a very weak timescale ratio

$$\frac{\tau_l}{\tau_{nl}^{m}} \sim P^{1/2} V_A^{-3/2} k_x^{-1} k_y \sim 3.3\,10^{-3} \ll 1. \tag{s16}$$